



HAL
open science

Light color acclimation is a key process in the global ocean distribution of *Synechococcus cyanobacteria*

Théophile Grébert, Hugo Doré, Frédéric Partensky, Gregory Farrant, Emmanuel Boss, Marc Picheral, Lionel Guidi, Stéphane Pesant, David J Scanlan, Patrick Wincker, et al.

► To cite this version:

Théophile Grébert, Hugo Doré, Frédéric Partensky, Gregory Farrant, Emmanuel Boss, et al.. Light color acclimation is a key process in the global ocean distribution of *Synechococcus cyanobacteria*. *Proceedings of the National Academy of Sciences of the United States of America*, 2018, 115 (9), pp.E2010-E2019. 10.1073/pnas.1717069115 . hal-01772758

HAL Id: hal-01772758

<https://hal.sorbonne-universite.fr/hal-01772758v1>

Submitted on 20 Apr 2018

HAL is a multi-disciplinary open access archive for the deposit and dissemination of scientific research documents, whether they are published or not. The documents may come from teaching and research institutions in France or abroad, or from public or private research centers.

L'archive ouverte pluridisciplinaire **HAL**, est destinée au dépôt et à la diffusion de documents scientifiques de niveau recherche, publiés ou non, émanant des établissements d'enseignement et de recherche français ou étrangers, des laboratoires publics ou privés.

1 **Light color acclimation: a key process in the global ocean**
2 **distribution of *Synechococcus* cyanobacteria**

3

4 Théophile Grébert^a, Hugo Doré^a, Frédéric Partensky^a, Gregory K. Farrant^{a,1}, Emmanuel S. Boss^b, Marc
5 Picheral^c, Lionel Guidi^c, Stéphane Pesant^{d,e}, David J. Scanlan^f, Patrick Wincker^g, Silvia G. Acinas^h, David
6 M. Kehoeⁱ and Laurence Garczarek^{a,2}

7 ^aSorbonne Universités-Université Paris 06 & Centre National de la Recherche Scientifique (CNRS),
8 UMR 7144, Marine Phototrophic Prokaryotes Team, Station Biologique, CS 90074, 29688 Roscoff
9 cedex, France; ^bMaine In-situ Sound and Color Lab, University of Maine, Orono, ME 04469; ^cSorbonne
10 Universités-Université Paris 06 & CNRS, UMR 7093, Observatoire océanologique, 06230 Villefranche-
11 sur-mer, France; ^dPANGAEA, Data Publisher for Earth and Environmental Science, University of
12 Bremen, Bremen, Germany; ^eMARUM, Center for Marine Environmental Sciences, University of
13 Bremen, Bremen, Germany; ^fUniversity of Warwick, School of Life Sciences, Coventry CV4 7AL, UK;
14 ^gCommissariat à l'Énergie Atomique et aux Énergies Alternatives (CEA), Institut de Génomique,
15 Genoscope, 91057 Evry, France; ^hDepartment of Marine Biology and Oceanography, Institute of
16 Marine Sciences (ICM), Consejo Superior de Investigaciones Científicas (CSIC), Barcelona ES-08003,
17 Spain; ⁱDepartment of Biology, Indiana University, Bloomington, IN 47405.

18 ¹Present address: Food Safety, Environment, and Genetics, Matís Ltd., 113 Reykjavík, Iceland.

19 ²To whom correspondence should be addressed. Email: laurence.garczarek@sb-roscoff.fr.

20

21 Classification: Biological Sciences/Environmental Sciences

22 Keywords: marine cyanobacteria, metagenomics, light quality, phycobilisome, *Tara* Oceans

23 Short title: Biogeography of *Synechococcus* pigment types

24 **Abstract**

25 Marine *Synechococcus* cyanobacteria are major contributors to global oceanic primary production
26 and exhibit a unique diversity of photosynthetic pigments, allowing them to exploit a wide range of
27 light niches. However, the relationship between pigment content and niche partitioning has
28 remained largely undetermined due to the lack of a single-genetic marker resolving all pigment types
29 (PTs). Here, we developed and employed a novel and robust method based on three distinct marker
30 genes (*cpcBA*, *mpeBA* and *mpeW*) to estimate the relative abundance of all known *Synechococcus*
31 PTs from metagenomes. Analysis of the *Tara* Oceans dataset allowed us, for the first time, to reveal
32 the global distribution of *Synechococcus* PTs and to define their environmental niches. Green-light
33 specialists (PT 3a) dominated in warm, green equatorial waters, whereas blue-light specialists (PT 3c)
34 were particularly abundant in oligotrophic areas. Type IV chromatic acclimators (CA4-A/B), which are
35 able to dynamically modify their light absorption properties to maximally absorb green or blue light,
36 were unexpectedly the most abundant PT in our dataset and predominated at depth and high
37 latitudes. We also identified populations in which CA4 might be nonfunctional due to the lack of
38 specific CA4 genes, notably in warm high-nutrient low-chlorophyll areas. Major ecotypes within
39 clades I-IV and CRD1 were preferentially associated with a particular PT, while others exhibited a
40 wide range of PTs. Altogether, this study provides important insights into the ecology of
41 *Synechococcus* and highlights the complex interactions between vertical phylogeny, pigmentation
42 and environmental parameters that shape *Synechococcus* community structure and evolution.

43

44 **Significance Statement**

45 Understanding the functional diversity of specific microbial groups at the global scale is critical yet
46 poorly developed. By combining the considerable knowledge accumulated through recent years on
47 the molecular bases of photosynthetic pigment diversity in marine *Synechococcus*, a major
48 phytoplanktonic organism, with the wealth of metagenomic data provided by the *Tara* Oceans

49 expedition, we have been able to reliably quantify all known pigment types along its transect and
50 provide the first global distribution map. Unexpectedly, cells able to dynamically change their
51 pigment content to match the ambient light color were ubiquitous and predominated in many
52 environments. Altogether, our results unveiled the role of adaptation to light quality on niche
53 partitioning in a key primary producer.

54

55 Introduction

56 Marine *Synechococcus* is the second most abundant phytoplankton group in the world's oceans and
57 constitutes a major contributor to global primary production and carbon cycling (1, 2). This genus
58 displays a wide genetic diversity and several studies have shown that among the ~20 clades defined
59 based on various genetic markers, five (clades I-IV and CRD1) predominate *in situ* and can be broadly
60 associated with distinct sets of physico-chemical parameters (3–5). In a recent study, we further
61 defined Ecologically Significant Taxonomic Units (ESTUs), i.e. organisms belonging to the same clade
62 and co-occurring in the field, and highlighted that the three main parameters affecting the *in situ*
63 distribution of these ESTUs were temperature and availability of iron and phosphorus (6). Yet, marine
64 *Synechococcus* also display a wide pigment diversity, suggesting that light could also influence their
65 ecological distribution, both qualitatively and quantitatively (7, 8).

66 This pigment diversity comes from differences in the composition of their main light-harvesting
67 antennae, called phycobilisomes (PBS; 7–9). These water-soluble macromolecular complexes consist
68 of a central core anchoring at least six radiating rods made of several distinct phycobiliproteins, i.e.
69 proteins to which specific enzymes (phycobilin lyases) covalently attach chromophores called
70 phycobilins (7, 10). Although the PBS core is conserved in all marine *Synechococcus*, rods have a very
71 variable composition, and three main pigment types (PTs) are usually distinguished (Fig. S1; 7, 11). In
72 PT 1, PBS rods are solely made of phycocyanin (PC, encoded by the *cpcBA* operon) and bear the red-
73 light absorbing phycocyanobilin (PCB; $A_{\max} = 620$ nm) as the sole chromophore. In PT 2, rods are
74 made of PC and phycoerythrin I (PE-I, encoded by *cpeBA*) and attach both PCB and the green-light
75 absorbing phycoerythrobilin (PEB; $A_{\max} = 550$ nm). All other marine *Synechococcus* belong to PT 3 and
76 have rods made of PC, PE-I and PE-II (encoded by *mpeBA*) that bind PCB, PEB and the blue-light
77 absorbing phycourobilin (PUB; $A_{\max} = 495$ nm; Fig. S1). Several subtypes can be defined within PT 3,
78 based on the fluorescence excitation ratio at 495 nm and 545 nm (hereafter $EX_{495:545}$; Fig. S1), a proxy
79 for the PUB:PEB ratio. This ratio is low ($EX_{495:545} < 0.6$) in subtype 3a (green light specialists),

80 intermediate in subtype 3b ($0.6 \leq \text{Ex}_{495:545} < 1.6$) and high ($\text{Ex}_{495:545} \geq 1.6$) in subtype 3c (blue light
81 specialists; 7, 11). Additionally, strains of subtype 3d are able to change their PUB:PEB ratio
82 depending on ambient light color, a process called type IV chromatic acclimation (hereafter CA4),
83 allowing them to maximally absorb blue or green light (11–14). Comparative genomic analyses
84 showed that genes involved in the synthesis and regulation of PBS rods are gathered into a dedicated
85 genomic region, the content and organization of which correspond to the different PTs (7). Similarly,
86 chromatic acclimation has been correlated with the presence of a small specific genomic island (CA4
87 genomic island) that exists in two distinct configurations (CA4-A and -B; 11). Both contain two
88 regulators (*fciA* and *fciB*) and a phycobilin lyase (*mpeZ* in CA4-A or *mpeW* in CA4-B), thus defining two
89 distinct CA4 genotypes: 3dA and 3dB (11, 14, 15). Finally, some strains possess a complete or partial
90 CA4 genomic island but are not able to perform CA4, displaying a fixed $\text{Ex}_{495:545}$ corresponding to 3a,
91 3b or 3c phenotypes (11).

92 As there is no correspondence between pigmentation and core genome phylogeny (7, 16, 17),
93 deciphering the relative abundance and niche partitioning of *Synechococcus* PTs in the environment
94 requires specific approaches. In the past 30 years, studies have been based either on i) proxies of the
95 PUB:PEB ratio as assessed by flow cytometry (18–20), fluorescence excitation spectra (21–27),
96 epifluorescence microscopy (28), or ii) phylogenetic analyses of *cpcBA* or *cpeBA* (17, 29–34). These
97 studies showed that PT 1 is restricted to and dominates in low salinity surface waters and/or
98 estuaries, which are characterized by a high turbidity resulting in a red wavelengths-dominated light
99 field (18, 22, 31–38), whereas PT 2 is found in coastal shelf waters or in the transition zones between
100 brackish and oceanic environments with intermediate optical properties (18, 27, 34, 36–39). Finally,
101 PT 3 with increasing PUB:PEB ratio are found over gradients from onshore mesotrophic waters,
102 characterized by green light dominance, to offshore oligotrophic waters, where blue light penetrates
103 the deepest (19–24, 28, 36, 38, 40). Some authors reported an increase in the PUB:PEB ratio with
104 depth (19, 21, 24), while others observed a constant ratio throughout the water column, a variability

105 potentially linked to the location, water column features and/or environmental parameters (22, 25,
106 28).

107 However, these analyses based on optical properties could only describe the distribution of
108 high- and low-PUB populations without being able to differentiate green (3a) or blue light (3c)
109 specialists from CA4 cells (3d) acclimated to green or blue light, while genetic analysis solely based on
110 *cpcBA* and/or *cpeBA* could not differentiate all PTs. For instance, only two studies have reported CA4
111 populations *in situ* either in the western English Channel (17) or in sub-polar waters of the western
112 Pacific Ocean (29) but none of them were able to differentiate CA4-B from high PUB (i.e. 3c)
113 populations. As a consequence, the global relative abundance of the different *Synechococcus* PTs,
114 particularly CA4, and the link between genetic and pigment diversity have remained largely unclear.

115 Here, we analyzed 109 metagenomic samples collected from all major oceanic basins during the
116 2.5-yr *Tara* Oceans (2009-2011) expedition (41) using a bioinformatic pipeline combining a
117 metagenomic read recruitment approach (6, 42) to recruit single reads from multiple PBS gene
118 markers and placement of these reads in reference trees to assign them to a given PT. This pipeline
119 allowed the first description of the worldwide distribution of all known *Synechococcus* PTs, as well as
120 of their realized environmental niches (*sensu* 43). This study provides a synoptic view of how a major
121 photosynthetic organism adapts to natural light color gradients in the ocean.

122 Results

123 A novel, robust approach for estimating pigment types abundance from metagenomes

124 We developed a multi-marker approach combining phylogenetic information retrieved from three
125 different genes or operons (*cpcBA*, *mpeBA* and *mpeW*; Fig. 1 and Datasets 1-2) to overcome the issue
126 of fully resolving the whole range of PTs. While *cpcBA* discriminated PT 1, 2 and 3 (Fig. 1A), only the
127 *mpeBA* operon, a PT 3 specific marker, was able to distinguish the different PT 3 subtypes (Fig. 1B),
128 though as for *cpeBA* it could not differentiate PT 3dB (CA4-B) from PT 3c (i.e. blue light specialists; 11,
129 29). The *mpeW* marker was thus selected to specifically target PT 3dB and, by subtraction,
130 enumerate PT 3c (Fig. 1C). Using the *cpcBA* marker, members of PT 2 were split into two well-defined
131 clusters, 2A and 2B (Fig. 1A), the latter corresponding to a purely environmental PT identified from
132 assembled metagenomes of the Baltic Sea (38). Strains KORDI-100 and CC9616 also clustered apart
133 from other strains in the *mpeBA* phylogeny, suggesting that they have a divergent evolutionary
134 history from other PT 3 members (Fig. 1B). This is supported by the diverged gene content and order
135 of their PBS rod genomic region and these strains were recently referred to as PT 3f, even though
136 they have a similar phenotype as PT 3c ($EX_{495:545}$ ratio ≥ 1.6 ; 30). To investigate the phylogenetic
137 resolution of small fragments of these three markers, sequences were removed one at a time from
138 the reference database, and simulated reads (150 bp long as compared to 164 bp in average for *Tara*
139 Oceans cleaned/merged reads) generated from this sequence were assigned using our bioinformatic
140 pipeline against a database comprising the remaining sequences. Inferred and known PTs were then
141 compared. The percentage of simulated reads assigned to the correct PT was between 93.2% and
142 97.0% for all three markers, with less than 2.1-5.6% of reads that could not be classified and an error-
143 rate below 2%, showing that all three markers display a sufficient resolution to reliably assign the
144 different PTs (Fig. S2B, D and F).

145 To ensure that the different markers could be quantitatively compared in a real dataset, we
146 examined the correlations between estimates of PT abundances using the different markers in the

147 109 metagenomes analyzed in this study. Total *cpcBA* counts were highly correlated ($R^2=0.994$,
148 $n=109$; Fig. S3A) with total *Synechococcus* counts obtained with the *petB* gene, which was previously
149 used to study the phylogeography of marine picocyanobacteria (6), and the correlation slope was not
150 significantly different from 1 (slope: 1.040; Wilcoxon's paired difference test p -value=0.356). *cpcBA* is
151 thus as good as *petB* at capturing the total population of *Synechococcus* reads. Moreover, counts of
152 *cpcBA* reads assigned to PT 3 and total *mpeBA* counts (specific for PT 3) were also strongly correlated
153 ($R^2=0.996$, $n=109$; Fig. S3B), and not skewed from 1 (slope of 0.991, Wilcoxon's p -value=0.607),
154 indicating that *mpeBA* and *cpcBA* counts can be directly compared. Although no redundant
155 information for PT 3dB is available with the three selected markers, another marker targeting 3dB
156 (*fciAB*) was tested and produced results similar to *mpeW* (Fig. S3C). These results demonstrate that
157 our multi-marker approach can be used to reliably and quantitatively infer the different
158 *Synechococcus* PTs from short metagenomic reads, with PT 1, 2A, 2B abundances being assessed by
159 *cpcBA* normalized counts, PT 3a, 3f and 3dA by *mpeBA* normalized counts, PT 3dB by *mpeW*
160 normalized counts and PT 3c by the difference between *mpeBA* normalized counts for 3c + 3dB and
161 *mpeW* normalized counts. We thus used this approach on the *Tara* Oceans metagenomes, generated
162 from 109 samples collected at 65 stations located in the major oceanic basins (Fig. 2).

163

164 **CA4 populations are widespread and predominate at depth and high latitudes**

165 The latitudinal distribution of *Synechococcus* inferred from *cpcBA* counts is globally consistent with
166 previous studies (2, 6, 44), with *Synechococcus* being present in most oceanic waters, but quasi
167 absent (< 20 *cpcBA* counts) beyond 60°S (Southern Ocean stations TARA_082 to TARA_085; Fig. 2B).
168 Overall, the number of recruited *cpcBA* reads per station was between 0 and 8,151 ($n=63$, median:
169 449, mean: 924, sd: 1478) for surface and 0 and 3,200 ($n=46$, median:170, mean: 446, sd: 664) for
170 deep chlorophyll maximum (DCM) samples, respectively. Stations with less than 30 *cpcBA* reads were
171 excluded from further analysis.

172 PT 1 and 2, being both known to be mostly found and abundant in coastal waters (29, 36, 38,
173 45), were expectedly almost absent from this dataset (total of 15 and 513 *cpcBA* reads, respectively;
174 Fig. 2A-B) since the *Tara* cruise sampling was principally performed in oceanic waters. While PT 2A
175 was mostly found at the surface at one station off Panama (TARA_141, 417 out of 6,637 reads at this
176 station; Fig. 2B), PT 2B was virtually absent (total of 3 *cpcBA* reads) from our dataset and might thus
177 be confined to the Baltic Sea (38). This low abundance of PT 1 and 2B precluded the correlation
178 analysis between their distribution and physico-chemical parameters. PT 3 was by far the most
179 abundant along the *Tara* Oceans transect, accounting for $99.1 \pm 1.4\%$ (mean \pm sd) of *cpcBA* reads at
180 stations with ≥ 30 *cpcBA* read counts. Interestingly, several PT 3 subtypes often co-occurred at a given
181 station.

182 PT 3a (green light specialists) totaled 20.3% of read counts, with similar abundance between
183 surface (20.5%) and DCM (19.4%) samples, and was particularly abundant in intertropical oceanic
184 borders and regional seas, including the Red Sea, the Arabian Sea and the Panama/Gulf of Mexico
185 area (Fig. 2B). Correlation analyses show that this PT is consistently associated with high
186 temperatures but also with greenish (as estimated from a low blue to green downwelling irradiance
187 ratio, $I_{495:545}$), particle-rich waters (high particle backscattering at 470 nm and beam attenuation
188 coefficient at 660 nm; Fig. 3). Still, in contrast with previous studies that reported the distribution of
189 low-PUB populations (19, 21, 23, 24, 26, 27), this PT does not seem to be restricted to coastal waters,
190 explaining its absence of correlation with chlorophyll concentration and colored dissolved organic
191 matter (cDOM).

192 Blue light specialists (PT 3c) appear to be globally widespread, with the exception of high
193 latitude North Atlantic waters, and accounted for 33.4% of reads, with a higher relative abundance at
194 the surface (36.8%) than at the DCM (23.3%, Fig. 2A). This PT is dominant in transparent,
195 oligotrophic, iron-replete areas such as the Mediterranean Sea as well as South Atlantic and Indian
196 Ocean gyres (Figs. 2B and 4C). In the South Pacific, PT 3c was also found to be predominant in the

197 Marquesas Islands area (TARA_123 and 124), where the coast proximity induced a local iron
198 enrichment (6). Consistently, PT 3c was found to be positively associated with iron concentration,
199 high temperature and DCM depth and anti-correlated with chlorophyll fluorescence, nitrogen
200 concentrations, net primary production (NPP) as well as other related optical parameters, such as
201 backscattering at 470 nm and beam attenuation coefficient at 660 nm (Fig. 3). Despite its rarity, PT 3f
202 seems to thrive in a similar environment, with the highest relative abundances in the Indian Ocean
203 and Mediterranean Sea (Figs. 2B and 4C). Its occurrence in the latter area might explain its strong
204 anti-correlation with phosphorus availability.

205 Both CA4 types, 3dA and 3dB, which represented 22.6% and 18.9% of reads respectively, were
206 unexpectedly widespread and could locally account for up to 95% of the total *Synechococcus*
207 population (Figs. 2, 4C and S4). In contrast to blue and green light specialists, both CA4 types were
208 proportionally less abundant at the surface (19.8% and 17.5%, for 3dA and 3dB, respectively) than at
209 depth (30.9% and 22.9%). Interestingly, PT 3dA and 3dB generally displayed complementary
210 distributions along the *Tara* Oceans transect (Fig. 2B). PT 3dA was predominant at high latitude in the
211 northern hemisphere as well as in other vertically mixed waters such as in the Chilean upwelling
212 (TARA_093) or in the Agulhas current (TARA_066 and 68; Fig 2B). Accordingly, PT 3dA distribution
213 seems to be driven by low temperature, high nutrient and highly productive waters (high NPP,
214 chlorophyll *a* and optical parameters), a combination of physico-chemical parameters almost
215 opposite to those observed for blue light specialists (PT 3c; Fig. 3). In contrast, PT 3dB shares a
216 number of characteristics with PT 3c, including the anti-correlation with nitrogen concentration and
217 association with iron availability (as indicated by both a positive correlation with [Fe] and negative
218 correlation with the iron limitation proxy Φ_{sat} ; Fig. 3), consistent with their widespread occurrence
219 in iron replete oceanic areas. Also noteworthy, PT 3dB was one of the sole PT (with 3f) to be
220 associated with low photosynthetically available radiation (PAR).

221

222 **Niche partitioning of *Synechococcus* populations rely on a subtle combination of ESTU and PT**
223 **niches**

224 We previously showed that temperature, iron and phosphorus availability constituted major factors
225 influencing the diversification and niche partitioning of *Synechococcus* ESTUs (i.e. genetically related
226 subgroups within clades that co-occur in the field; 6). Yet, these results cannot be extended to PTs
227 since the pigment content does not follow the vertical phylogeny (7). In order to decipher the
228 respective roles of genetic and pigment diversity in *Synechococcus* community structure, we
229 examined the relationships between ESTUs and PTs *in situ* abundances through correlation and
230 NMDS analyses (Fig. 4A-B) and compared their respective distributions (Figs. 4C and S4).

231 Interestingly, all PTs are either preferentially associated with or excluded from a subset of
232 ESTUs. PT 2A is found at low abundance at a few stations along the *Tara* Oceans transect and, when
233 present, it is seemingly associated with the rare ESTU 5.3B (Fig. 4A), an unusual PT/ESTU combination
234 so far only observed in metagenomes from freshwater reservoirs (46). PT 3a is associated with ESTUs
235 EnvBC (occurring in low iron areas) and IIA, the major ESTU in the global ocean (Fig. 4A), a result
236 consistent with NMDS analysis, which shows that PT 3a is found in assemblages dominated by these
237 two ESTUs (indicated by red and grey backgrounds in Fig. 4B), as well as with independent
238 observations on cultured strains (Dataset 3). PT 3c is associated with ESTU IIIA (the dominant ESTU in
239 P-depleted areas), as observed on many isolates (Dataset 3), and is also linked, like PT 3f, with ESTUs
240 IIIB and WPC1A, both present at lower abundance than IIIA in P-poor waters (Fig. 4A). PT 3f is also
241 associated with the newly described and low-abundance ESTU XXA (previously EnvC; Fig. S5; 4, 6).
242 Both PT 3f and ESTU XXA were rare in our dataset but systematically co-occurred, in agreement with
243 the fact that the only culture representative of the latter clade belongs to PT 3f (Dataset 3).

244 PT 3dA appears to be associated with all ESTUs from clades CRD1 (specific to iron-depleted
245 areas) as well as with those representative of coastal and cold waters (IA, IVA, IVC), but is anti-
246 correlated with most other major ESTUs (IIA, IIIA and -B, WPC1A and 5.3B; Fig. 4A). This pattern is

247 opposite to PT 3dB that is preferentially found associated with ESTU IIA, IIB and 5.3A, but not in
248 CRD1A or -C (Fig. 4A). Thus, it seems that the two types of CA4 are found in distinct and
249 complementary sets of ESTUs. Interestingly, our analysis might suggest the occurrence of additional
250 PTs not isolated so far, since a number of reads (0.7% and 2.7% of *cpcBA* and *mpeBA* counts,
251 respectively, Fig. 2A) could not be assigned to any known PTs. For instance, while most CRD1C seem
252 preferentially associated with PT 3dA, a fraction of the population could only be assigned at the PT 3
253 level (Fig. 4A). Similarly, a number of reads could not be assigned to any known PT in stations rich in
254 ESTU 5.3A and XXA, although one cannot exclude that this observation might be due to a low number
255 of representative strains, and thus PT reference sequences, for these ESTUs.

256 The preferred association of PTs with specific ESTUs is also well illustrated by some concomitant
257 shifts of PTs and ESTU assemblages. For instance, in the wintertime North Atlantic Ocean, the shift
258 from 3dB-dominated stations on the western side (TARA_142 and TARA_146-149) to 3dA-dominated
259 stations near European coasts (TARA_150 to 152) and North of Gulf stream (TARA_145) is probably
260 related to the shift in ESTU assemblages occurring along this transect, with ESTU IIA being gradually
261 replaced by ESTU IVA (Fig. 4C; see also 6). Similarly, the takeover of CRD1C by IIA in the Marquesas
262 Island area (TARA_123 to 125), which is iron-enriched with regard to surrounding high-nutrient low-
263 chlorophyll (HNLC) waters (TARA_122 and 128), perfectly matched the corresponding replacement of
264 PT 3dA by 3c. However, in several other cases, PT shifts were not associated with a concomitant
265 ESTU shift or vice versa. One of clearest examples of these dissociations is the transect from the
266 Mediterranean Sea to the Indian Ocean, where the entry in the northern Red Sea through the Suez
267 Canal triggered a sharp shift from a IIIA- to a IIA-dominated community (TARA_030 and 031), which
268 was not accompanied by any obvious change in PTs. Conversely, a sharp rise in the relative
269 abundance of PT 3a was observed in the southern Red Sea/northeastern Indian Ocean (TARA_033 to
270 038) without changes in the large dominance of ESTU IIA. Altogether, this strongly suggests that a
271 subtle combination of ESTUs and PTs respective niche occupancy is responsible for the observed
272 niche partitioning of *Synechococcus* populations.

273

274 **Deficient chromatic acclimators are dominant in HNLC areas**

275 Although our results clearly indicate that CA4 cells represent a large proportion of the *Synechococcus*
276 community in a wide range of ecological niches, this must be somewhat tempered by the fact that, in
277 culture, about 30% of the strains possessing a CA4-A or B genomic island are not able to
278 chromatically acclimate (Dataset 3; 11). Some of these natural mutants have an incomplete CA4
279 genomic island (Fig. S6K). For example, strains WH8016 (ESTU IA) and KORDI-49 (WPC1A) both lack
280 the CA4-A specific lyase-isomerase MpeZ, an enzyme shown to bind a PUB molecule on PE-II (14),
281 and display a green light specialist phenotype (PT 3a, $EX_{495:545} \sim 0.4$) whatever the ambient light color
282 (11). However, since they possess a PT 3a *mpeBA* allele, reads from field WH8016- or KORDI-49-like
283 cells are adequately counted as PT 3a (Fig. S6K). Another CA4-deficient strain, BIOS-E4-1 (ESTU
284 CRD1C), possesses *mpeZ* and a 3dA *mpeBA* allele but lacks the CA4 regulators FciA and FciB as well as
285 the putative lyase MpeY and exhibits a fixed blue light specialist phenotype (PT 3c, $EX_{495:545} \sim 1.7$; Fig.
286 S6K; 11, 15). Thus, reads from such natural *Synechococcus* CA4-incapable mutants in the field are
287 counted as 3dA using the *mpeBA* marker. Lastly, the strain MVIR-18-1 possesses a complete CA4-A
288 island and a 3dA *mpeBA* allele but lacks *mpeU*, a gene necessary for blue light acclimation (Fig. S6K;
289 47). While MVIR-18-1 displays a fixed green light phenotype, reads from such *Synechococcus* are also
290 erroneously counted as 3dA.

291 To assess the significance of these genotypes in the field, we compared the normalized read
292 counts obtained for 3dA with *mpeBA*, *fciAB*, *mpeZ*, *mpeU* and *mpeY* (Fig. S6A-J). Overall this analysis
293 revealed a high consistency between these different markers ($0.860 < R^2 < 0.986$), indicating that most
294 *mpeZ*-containing populations also contained 3dA alleles for *fciAB*, *mpeY*, *mpeU* and *mpeBA* and are
295 therefore likely able to perform CA4. However, a number of stations, all located in HNLC areas
296 (TARA_094, 111 and 122 to 128 in the Pacific Ocean and TARA_052 located northwest of
297 Madagascar, Fig. 2B), displayed more than 10-fold higher *mpeBA*, *mpeU* and *mpeZ* counts than *fciAB*

298 and *mpeY* counts (Fig. S6A, B, E, F, H, I). This indicates that a large proportion or even the whole
299 population (TARA_122 and 124) of 3dA in these HNLC areas is probably lacking the *FciA/B* regulators
300 and *MpeY* and, like strain BIOS-E4-1 (Fig. S6K), might thus be stuck in the blue light specialist
301 phenotype (PT 3c; 11). Conversely, station TARA_067 exhibited consistently more than twice the
302 *fciAB* and *mpeZ* counts compared to *mpeBA*, *mpeY* or *mpeU* (Fig. S6B-E, G, H) and was a clear outlier
303 when comparing pigment type and clade composition (Fig. S7). This suggests that the proportion of
304 PT 3dA might have been underestimated at this station, as a significant proportion of this population
305 probably corresponds to PT 3a genotypes that have acquired a CA4-A island by lateral gene transfer,
306 as is seemingly the case for strains WH8016 and KORDI-49. Finally, no station exhibited markedly
307 lower *mpeU* counts compared to all other genes, indicating that the genotype of strain MVIR-18-1 is
308 probably rare in the oceans.

309 It must be noted that two out of the six sequenced CA4-B strains (WH8103 and WH8109) also
310 have a deficient CA4 phenotype and display a constant, intermediate $EX_{495:545}$ ratio (0.7 and 1,
311 respectively), despite any obvious PBS- or CA4-related gene deletion (11). Accordingly, the plot of
312 3dB normalized read counts obtained with *mpeW* vs. *fciAB* shows no clear outlier (Fig. S3C).

313

314 Discussion

315 Marine *Synechococcus* display a large pigment diversity, with different PTs preferentially harvesting
316 distinct regions of the light spectrum. Previous studies based on optical properties or on a single
317 genetic marker could not differentiate all PTs (17, 29–31), and thus neither assess their respective
318 realized environmental niches (43) nor the role of light quality on the relative abundance of each PT.
319 Here, we showed that a metagenomic read recruitment approach combining three genetic markers
320 can be used to reliably predict all major PTs. Applied to the extensive *Tara* Oceans dataset, this
321 original approach, which avoids PCR amplification and cloning biases, allowed us to describe for the

322 first time the distribution of the different *Synechococcus* PTs at the global scale and to refine our
323 understanding of their ecology.

324 PT 3 was found to be largely dominant over PT 1 and 2 along the oceanic *Tara* Oceans transect,
325 in agreement with the coastal-restricted distribution of the latter PTs (18, 22, 27, 31–34, 37–39).
326 Biogeography and correlation analyses with environmental parameters provided several novel and
327 important insights concerning niche partitioning of PT 3 subtypes. Green (PT 3a) and blue (PT 3c)
328 light specialists were both shown to dominate in warm areas but display clearly distinct niches, with
329 3a dominating in *Synechococcus*-rich stations located on oceanic borders, while 3c predominated in
330 purely oceanic areas where the global abundance of *Synechococcus* is low. These results are in
331 agreement with the prevailing view of an increase in the PUB:PEB ratio from green onshore
332 mesotrophic waters to blue offshore oligotrophic waters (19–24, 26–29, 40, 48). Similarly, we
333 showed that PT 3dB, which could not be distinguished from PT 3c in previous studies (17, 29–31),
334 prevails in more coastal and/or mixed temperate waters than do 3c populations. The realized
335 environmental niche of the second type of CA4 (PT 3dA) is the best defined of all PTs as it is clearly
336 associated with nutrient-rich waters and with the coldest stations of our dataset, occurring at high
337 latitude, at depth and/or in vertically mixed waters (e.g., TARA_068, 093 and 133). This result is
338 consistent with a recent study demonstrating the dominance of 3dA in sub-Arctic waters of the
339 Northwest Pacific Ocean (29), suggesting that the prevalence of 3dA at high latitude can be
340 generalized. The decrease of PT 3c (blue light specialists) with depth is unexpected given previous
341 reports of a constant (22, 25, 28, 49) or increasing (19, 21, 24) PUB:PEB ratio throughout the water
342 column. However, the high abundance of CA4 can reconcile these observations with the decreased
343 abundance of PT 3c, as cells capable of CA4 likely have a blue-light phenotype at depth. Altogether,
344 while little was previously known about the abundance and distribution of CA4 populations in the
345 field, here we show that they are ubiquitous, dominate in a wide range of niches, are present both in
346 coastal and oceanic mixed waters, and overall are the most abundant *Synechococcus* PT.

347 The relationship between ESTUs and PTs shows that some ESTUs are preferentially associated
348 with only one PT, while others present a much larger pigment diversity. ESTU IIA, the most abundant
349 and ubiquitous ESTU in the field (5, 6), displays the widest PT diversity (Fig. 4B), a finding confirmed
350 by clade II isolates spanning the largest diversity of pigment content, with representative strains of
351 PT 2, 3a, 3c and 3dB within this clade (Dataset 3; see also 7, 11, 50–52). This suggests that this ESTU
352 can colonize all light color niches, an ability which might be partially responsible for its global
353 ecological success. Our current results do not support the previously observed correlation between
354 clade III and PT 3a (29) since the two ESTUs defined within this clade (IIIA and B) were associated
355 with PT 3c and/or 3f. This discrepancy could be due either to the different methods used in these
356 studies or to the occurrence of genetically distinct clade III populations in coastal areas of the
357 northwestern Pacific Ocean and along the *Tara* Oceans transect. However, the pigment phenotype of
358 strains isolated to date is more consistent with our findings (Dataset 3; 16, 36).

359 In contrast to most other PTs, the association between PT 3dA and ESTUs was found to be nearly
360 exclusive in the field, as ESTUs from clades I, IV, CRD1 and EnvA were not associated with any other
361 PT, and reciprocally PT 3dA is only associated with these clades (Fig. 4A). An interesting exception to
362 this general rule was observed in the Benguela upwelling (TARA_067), where the dominant ESTU IA
363 population both displays a 3a *mpeBA* allele and possesses *fcIA/B* and *mpeZ* genes (Figs. S6K and S7),
364 suggesting that cells, which were initially green light specialists (PT 3a), have inherited a complete
365 CA4-A island through lateral gene transfer at this station. Interestingly, among the seven clade I
366 strains sequenced to date, three possess a 3a *mpeBA* allele, among which WH8016 also has a CA4-A
367 island but only partial (lacking *mpeZ*) and therefore not functional (11). It is thus difficult to conclude
368 whether the lateral transfer of this island, likely a rare event since it was only observed in
369 populations of the Benguela upwelling, has conferred these populations the ability to perform CA4.

370 Another important result of this study was the unsuspected importance of populations that
371 have likely lost the ability to chromatically acclimate, specifically in warm HNLC areas, which cover

372 wide expanses of the South Pacific Ocean (53). Interestingly, populations living in these ultra-
373 oligotrophic environments have a different genetic basis for their consistently elevated PUB
374 phenotype than do typical blue light specialists (i.e. PT 3c), since they have lost the CA4 regulators
375 *fciA/B* and accumulated mutations in *mpeY*, a yet uncharacterized member of the phycobilin lyase
376 family, as observed in strain BIOS-E4-1 (Fig. S6K; 11). This finding, consistent with the previous
377 observation that the south Pacific is dominated by high-PUB *Synechococcus* (22), is further supported
378 by the recent sequencing of three isolates from the Equatorial Pacific, strains MITS9504, MITS9509
379 (both CRD1C) and MITS9508 (CRD1A; 54), all of which contain, like BIOS-E4-1, a 3dA *mpeBA* allele, a
380 CA4-A island lacking *fciA/B* and a partial (MITS9508) or highly degenerated (2 other MIT strains)
381 *mpeY* gene sequence (Fig. S6K). Thus, these natural CA4-A mutants seem to have adapted to blue,
382 ultra-oligotrophic waters by inactivating a likely energetically costly acclimation mechanism (positive
383 selection), although we cannot exclude that it might be a consequence of the lower selection
384 efficiency associated to the reduced effective population size of *Synechococcus* in such an extreme
385 environment (genetic drift). If, as we hypothesize, all *Synechococcus* cells counted as 3dA at these
386 stations are CA4-deficient, these natural mutants would represent about 15% of the total 3dA
387 population. In contrast, CRD1-A populations of the eastern border of the Pacific Ocean (TARA_102,
388 109-110, 137) are likely true CA4 populations as they possess all CA4 genes (Fig. S6K).

389 In conclusion, our study provided novel insights into the distribution, ecology and adaptive value
390 of all known *Synechococcus* PTs. Unexpectedly, the sum of 3dA and 3dB constituted about 40% of the
391 total *Synechococcus* counts in the *Tara* Oceans dataset, making chromatic acclimators (PT 3d) the
392 most globally abundant PT, even when taking into account potential CA4-deficient natural mutants.
393 In addition, this PT made up 95% of the *Synechococcus* population at high latitudes and was present
394 in every one of the five major clades in the field (I, II, III, IV and CRD1). This suggests that chromatic
395 acclimation likely confers a strong adaptive advantage compared to strains with a fixed
396 pigmentation, particularly in vertically mixed environments and at depth at stations with a stratified
397 water column. The occurrence of natural CA4 mutants and evidence for lateral transfer of the CA4

398 genomic island further support previous hypotheses that not only temperature and nutrient
399 availability (3, 5, 6) but also light quality (7, 52) co-exert selective pressures affecting marine
400 *Synechococcus* evolution. Thus, changes in pigment diversity could occur in response to changes in
401 light niches by acquisition or loss of specific PBS synthesis and/or regulation genes, as previously
402 observed for phosphorus and nitrogen transport genes in *Prochlorococcus* (55–57). Still, the complex
403 interactions between PTs, vertical phylogeny and environmental parameters remain unclear and
404 more work is needed to refine our understanding of the balance between the forces shaping
405 community composition and *Synechococcus* evolution. At the boundaries of *Synechococcus*
406 environmental niche(s), where the harshest conditions are encountered, both pigment and clade
407 diversity are drastically reduced, and this concomitant reduction tends to support a co-selection by
408 light quality and other environmental parameters. On the contrary, the diverse PTs occurring within
409 some clades, as well as the co-occurrence of different PTs at most stations compared to more clear-
410 cut clade shifts (e.g., in the Red Sea/Indian Ocean) might indicate that light quality is not the
411 strongest selective force or that light changes are too transient to allow the dominance and fixation
412 of a particular PT in a population. Future experimental work exploring the fitness of distinct ESTU/PT
413 combinations under different controlled environmental conditions (including temperature, nutrients
414 and light) might help clarifying the respective effects of these parameters on the diversification of
415 this ecologically important photosynthetic organism.

416

417 **Materials and Methods**

418 **Metagenomic samples**

419 This study focused on 109 metagenomic samples corresponding to 65 stations from the worldwide
420 oceans collected during the 2.5-yr *Tara* Oceans circumnavigation (2009-2011). Water sample and
421 sequence processing are the same than in (6). Dataset 4 describes all metagenomic samples with

422 location and sequencing effort. Sequencing depths ranged from 16×10^6 to 258×10^6 reads per
423 sample after quality control and paired-reads merging, and corresponding fragments lengths
424 averaged 164 ± 20 bp (median: 168 bp).

425

426 **Databases: reference and outgroup sequences**

427 A reference database comprising the full-length gene or operon nucleotide sequences was generated
428 for each marker used in this study (*cpcBA*, *mpeBA* and *mpeW*) based on culture isolates with
429 characterized pigment type (Dataset 1). These databases comprised 83 *cpcBA* sequences (64 unique),
430 including 18 PT 1, 5 PT 2A, 19 PT 2B and 39 PT 3, 41 *mpeBA* sequences (all unique), including 11 PT
431 3a, 2 PT 3f, 11 PT 3dA and 17 PT 3dB and 5 unique *mpeW* sequences. For each marker, a reference
432 alignment was generated with MAFFT L-INS-i v6.953b (58), and a reference phylogenetic tree was
433 inferred with PhyML v. 20120412 (GTR+I+G, 10 random starting trees, best of SPR and NNI moves,
434 500 bootstraps; (59) and drawn using the ETE Toolkit (60).

435 A database of outgroups was also built, comprising paralogous sequences from marine
436 *Synechococcus* or *Prochlorococcus* as well as orthologous sequences from other marine and
437 freshwater organisms retrieved from public databases. For *cpcBA* and *mpeBA*, the outgroup
438 databases comprised *apcA*, *apcB*, *apcD*, *apcF* and *cpeBA* from marine *Synechococcus*, *ppeBA* from
439 *Prochlorococcus*, *cpcBA* and *cpeBA* from other non-picocyanobacterial organisms as well as either
440 *mpeBA* or *cpcBA* from marine *Synechococcus*, respectively (Datasets 1-2). For *mpeW*, the outgroup
441 database was made of paralogous genes (*mpeZ*, *mpeY* and *cpeY*) from marine *Synechococcus* or
442 *Prochlorococcus*, as no ortholog could be identified in public databases. Similarly, for *mpeY* and
443 *mpeZ*, the outgroup database comprised *cpeY*, *mpeW* as well as *mpeZ* or *mpeY*, respectively. The
444 outgroup database for *mpeU* comprised *cpeF* paralogous sequences from marine *Synechococcus* and
445 *Prochlorococcus*. No outgroup database was used for *fciAB*, as no paralogs or other distantly related
446 sequences were found either in marine *Synechococcus* and *Prochlorococcus* or in public databases.

447

448 **Read assignation and estimation of PT abundance**

449 Reads were preselected using BLAST+ (61) with relaxed parameters (blastn, maximum E-value of 1e-
450 5, minimum percent identity 60%, minimum 75% of read length aligned), using reference sequences
451 as subjects; the selection was then refined by a second BLAST+ round against databases of
452 outgroups: reads with a best-hit to outgroup sequences were excluded from downstream analysis.
453 Selected reads were then aligned to the marker reference alignment with MAFFT v.7.299b (--
454 addfragments --adjustdirectionaccurately) and placed in the marker reference phylogenetic tree with
455 *pplacer* (62). For each read, *pplacer* returns a list of possible positions (referred to as placements) at
456 which it can be placed in the tree and their associated “likelihood weight ratio” (LWR, proxy for the
457 probability of the placement; see *pplacer* publication and documentation for more details). Reads
458 were then assigned to a pigment type using a custom classifier written in Python. Briefly, internal
459 nodes of the reference tree were assigned a pigment type based on the pigmentation of descending
460 nodes (PT of child reference sequences if the same for all of them, “unclassified” otherwise). For
461 each read, placements were assigned to their nearest ascending or descending node based on their
462 relative position on the edge, and the lowest common ancestor (LCA) of the set of nodes for which
463 the cumulated LWR was greater than 0.95 (LCA of possible placements at 95% probability) was then
464 computed. Finally, the read was assigned to the pigment type of this LCA. Different combinations of
465 read assignment parameters (LCA at 90%, 95% or 100%; assignation of placements to the ascending,
466 descending or nearest node) were also assessed, and resulted either in higher rates of unassigned
467 reads or of wrongly assigned reads (Fig. S2).

468 Read counts were normalized by adjusted marker length: for each marker and each sequence
469 file, counts were normalized by $(L - \ell + 1)$, with L the length of the marker gene (*cpcBA* mean length:
470 1053.7 bp; *mpeBA* mean length: 1054.6 bp; *mpeW* mean length: 1193.3 bp) and ℓ the mean length of
471 reads in the sequence file. Finally, the abundance of PT 1, 2A and 2B was defined as the normalized

472 *cpcBA* read counts of these PT, the abundance of PT 3a, 3f and 3dA as the normalized *mpeBA* read
473 counts of these PT, 3dB as the normalized *mpeW* count and 3c as the difference between the
474 normalized *mpeBA* (3c + 3dB) read count and the PT 3dB count assessed with *mpeW*. The abundance
475 of unclassified sequences was also taken into account. Detailed *petB* counts for clade and ESTU
476 abundances were obtained from (6).

477

478 **Read assignment simulations**

479 For each marker, simulated reads were generated from one reference sequence at a time using a
480 sliding window of 100, 125 or 150 bp (*Tara* Oceans mean read length: 164.2 bp; median 169 bp) and
481 steps of 5 bp. Simulated reads were then assigned to a pigment type with the aforementioned
482 bioinformatic pipeline, using all reference sequences except the one used to simulate reads (“leave
483 one out” cross-validation scheme). Inferred PTs of simulated fragments were then compared to
484 known PTs of reference sequences.

485

486 **Statistical analyses**

487 All environmental parameters used for statistical analyses are the same as in (6), except the blue to
488 green irradiance ratio that was modeled as described in the supplementary materials and methods.
489 Hierarchical clustering and NMDS analyses of stations were performed using R (63) packages cluster
490 v1.14.4 (64) and MASS v7.3–29 (65), respectively. PT contingency tables were filtered by considering
491 only stations with more than 30 *cpcBA* reads and 30 *mpeBA* reads, and only PT appearing in at least
492 two stations and with more than 150 reads in the whole dataset. Contingency tables were
493 normalized using Hellinger transformation that gives lower weights to rare PT. The Bray–Curtis
494 distance was then used for ordination (isoMDS function; maxit, 100; k, 2). Correlations were

495 performed with R package Hmisc_3.17-4 with Benjamini & Hochberg multiple comparison adjusted
496 p-value (66).

497

498 **Acknowledgements**

499 We warmly thank Dr. Annick Bricaud for fruitful discussions on biooptics, members of the ABiMS
500 platform (Roscoff) for providing us an efficient storage and computing facility for our bioinformatics
501 analyses as well as the NERC Biomolecular Analysis Facility (NBAF, Centre for Genomic Research,
502 University of Liverpool) for sequencing some *Synechococcus* genomes used in this study. This work
503 was supported by the French “Agence Nationale de la Recherche” Programs SAMOSA (ANR-13-ADAP-
504 0010) and France Génomique (ANR-10-INBS-09), the French Government “Investissements d'Avenir”
505 programs OCEANOMICS (ANR-11-BTBR-0008), the European Union's Seventh Framework Programs
506 FP7 MicroB3 (grant agreement 287589) and MaCuMBA (grant agreement 311975), UK Natural
507 Environment Research Council Grant NE/I00985X/1 and the Spanish Ministry of Science and
508 Innovation grant MicroOcean PANGENOMICS (GL2011-26848/BOS). We also thank the support and
509 commitment of the *Tara* Oceans coordinators and consortium, Agnès b. and E. Bourgois, the Veolia
510 Environment Foundation, Région Bretagne, Lorient Agglomeration, World Courier, Illumina, the EDF
511 Foundation, FRB, the Prince Albert II de Monaco Foundation, the *Tara* schooner and its captains and
512 crew. *Tara* Oceans would not exist without continuous support from 23 institutes
513 (<http://oceans.taraexpeditions.org>). This article is contribution number XXXX of *Tara* Oceans.

514

515 **References**

- 516 1. Guidi L, et al. (2016) Plankton networks driving carbon export in the oligotrophic ocean. *Nature*
517 532(7600):465–470.
- 518 2. Flombaum P, et al. (2013) Present and future global distributions of the marine Cyanobacteria
519 *Prochlorococcus* and *Synechococcus*. *Proc Natl Acad Sci USA* 110(24):9824–9829.
- 520 3. Zwirgmaier K, et al. (2008) Global phylogeography of marine *Synechococcus* and
521 *Prochlorococcus* reveals a distinct partitioning of lineages among oceanic biomes. *Environ*
522 *Microbiol* 10(1):147–161.
- 523 4. Mazard S, Ostrowski M, Partensky F, Scanlan DJ (2012) Multi-locus sequence analysis,
524 taxonomic resolution and biogeography of marine *Synechococcus*. *Environ Microbiol* 14(2):372–
525 386.
- 526 5. Sohm JA, et al. (2016) Co-occurring *Synechococcus* ecotypes occupy four major oceanic regimes
527 defined by temperature, macronutrients and iron. *ISME J* 10(2):333–345.
- 528 6. Farrant GK, et al. (2016) Delineating ecologically significant taxonomic units from global
529 patterns of marine picocyanobacteria. *Proc Natl Acad Sci USA* 113(24):E3365–E3374.
- 530 7. Six C, et al. (2007) Diversity and evolution of phycobilisomes in marine *Synechococcus* spp.: a
531 comparative genomics study. *Genome Biol* 8(12):R259.
- 532 8. Alberte RS, Wood AM, Kursar TA, Guillard RRL (1984) Novel phycoerythrins in marine
533 *Synechococcus* spp. *Plant Physiol* 75(3):732–739.
- 534 9. Ong LJ, Glazer AN (1991) Phycoerythrins of marine unicellular cyanobacteria. I. Bilin types and
535 locations and energy transfer pathways in *Synechococcus* spp. phycoerythrins. *J Biol Chem*
536 266(15):9515–9527.
- 537 10. Sidler WA (1994) Phycobilisome and phycobiliprotein structures. *The Molecular Biology of*
538 *Cyanobacteria*, Advances in Photosynthesis. (Springer, Dordrecht), pp 139–216.
- 539 11. Humily F, et al. (2013) A gene island with two possible configurations is involved in chromatic
540 acclimation in marine *Synechococcus*. *PLoS ONE* 8(12):e84459.

- 541 12. Palenik B (2001) Chromatic adaptation in marine *Synechococcus* strains. *Appl Environ Microbiol*
542 67(2):991–994.
- 543 13. Everroad C, et al. (2006) Biochemical cases of type IV chromatic adaptation in marine
544 *Synechococcus* spp. *J Bacteriol* 188(9):3345–3356.
- 545 14. Shukla A, et al. (2012) Phycoerythrin-specific bilin lyase-isomerase controls blue-green
546 chromatic acclimation in marine *Synechococcus*. *Proc Natl Acad Sci USA* 109(49):20136–20141.
- 547 15. Sanfilippo JE, et al. (2016) Self-regulating genomic island encoding tandem regulators confers
548 chromatic acclimation to marine *Synechococcus*. *Proc Natl Acad Sci USA* 113(21):6077–6082.
- 549 16. Toledo G, Palenik B, Brahamsha B (1999) Swimming marine *Synechococcus* strains with widely
550 different photosynthetic pigment ratios form a monophyletic group. *Appl Environ Microbiol*
551 65(12):5247–5251.
- 552 17. Humily F, et al. (2014) Development of a targeted metagenomic approach to study a genomic
553 region involved in light harvesting in marine *Synechococcus*. *FEMS Microbiol Ecol* 88(2):231–
554 249.
- 555 18. Jiang T, et al. (2016) Temporal and spatial variations of abundance of phycocyanin- and
556 phycoerythrin-rich *Synechococcus* in Pearl River Estuary and adjacent coastal area. *J Ocean Univ*
557 *China* 15(5):897–904.
- 558 19. Olson RJ, Chisholm SW, Zettler ER, Armbrust EV (1990) Pigments, size, and distributions of
559 *Synechococcus* in the North Atlantic and Pacific Oceans. *Limnol Oceanogr* 35(1):45–58.
- 560 20. Sherry ND, Wood AM (2001) Phycoerythrin-containing picocyanobacteria in the Arabian Sea in
561 february 1995: diel patterns, spatial variability, and growth rates. *Deep Sea Res Part II* 48(6–
562 7):1263–1283.
- 563 21. Lantoine F, Neveux J (1997) Spatial and seasonal variations in abundance and spectral
564 characteristics of phycoerythrins in the tropical northeastern Atlantic Ocean. *Deep Sea Res Part*
565 *I* 44(2):223–246.
- 566 22. Neveux J, Lantoine F, Vaultot D, Marie D, Blanchot J (1999) Phycoerythrins in the southern
567 tropical and equatorial Pacific Ocean: evidence for new cyanobacterial types. *J Geophys Res*
568 *Oceans* 104(C2):3311–3321.

- 569 23. Campbell L, et al. (1998) Response of microbial community structure to environmental forcing
570 in the Arabian Sea. *Deep Sea Res Part II* 45(10):2301–2325.
- 571 24. Wood AM, Lipsen M, Coble P (1999) Fluorescence-based characterization of phycoerythrin-
572 containing cyanobacterial communities in the Arabian Sea during the Northeast and early
573 Southwest Monsoon (1994–1995). *Deep Sea Res Part II* 46(8):1769–1790.
- 574 25. Yona D, Park MO, Oh SJ, Shin WC (2014) Distribution of *Synechococcus* and its phycoerythrin
575 pigment in relation to environmental factors in the East Sea, Korea. *Ocean Sci J* 49(4):367–382.
- 576 26. Hoge FE, Wright CW, Kana TM, Swift RN, Yungel JK (1998) Spatial variability of oceanic
577 phycoerythrin spectral types derived from airborne laser-induced fluorescence emissions. *Appl*
578 *Opt* 37(21):4744–4749.
- 579 27. Wood AM, Phinney DA, Yentsch CS (1998) Water column transparency and the distribution of
580 spectrally distinct forms of phycoerythrin- containing organisms. *Mar Ecol Prog Ser* 162:25–31.
- 581 28. Campbell L, Iturriaga R (1988) Identification of *Synechococcus* spp. in the Sargasso Sea by
582 immunofluorescence and fluorescence excitation spectroscopy performed on individual cells.
583 *Limnol Oceanogr* 33(5):1196–1201.
- 584 29. Xia X, et al. (2017) Phylogeography and pigment type diversity of *Synechococcus* cyanobacteria
585 in surface waters of the northwestern pacific ocean. *Environ Microbiol* 19(1):142–158.
- 586 30. Xia X, Liu H, Choi D, Noh JH (2017) Variation of *Synechococcus* pigment genetic diversity along
587 two turbidity gradients in the China Seas. *Microb Ecol*:1–12.
- 588 31. Xia X, Guo W, Tan S, Liu H (2017) *Synechococcus* assemblages across the salinity gradient in a
589 salt wedge estuary. *Front Microbiol* 8:32. Liu H, Jing H, Wong THC, Chen B (2014) Co-
590 occurrence of phycocyanin- and phycoerythrin-rich *Synechococcus* in subtropical estuarine and
591 coastal waters of Hong Kong: PE-rich and PC-rich *Synechococcus* in subtropical coastal waters.
592 *Environ Microbiol Rep* 6(1):90–99.
- 593 33. Chung C-C, Gong G-C, Huang C-Y, Lin J-Y, Lin Y-C (2015) Changes in the *Synechococcus*
594 assemblage composition at the surface of the East China Sea due to flooding of the Changjiang
595 river. *Microb Ecol* 70(3):677–688.
- 596 34. Haverkamp T, et al. (2008) Diversity and phylogeny of Baltic Sea picocyanobacteria inferred
597 from their ITS and phycobiliprotein operons. *Environ Microbiol* 10(1):174–188.

- 598 35. Stomp M, et al. (2007) Colourful coexistence of red and green picocyanobacteria in lakes and
599 seas. *Ecol Lett* 10(4):290–298.
- 600 36. Hunter-Cevera KR, Post AF, Peacock EE, Sosik HM (2016) Diversity of *Synechococcus* at the
601 Martha's Vineyard Coastal Observatory: insights from culture isolations, clone libraries, and
602 flow cytometry. *Microb Ecol* 71(2):276–289.
- 603 37. Fuller NJ, et al. (2003) Clade-specific 16S ribosomal DNA oligonucleotides reveal the
604 predominance of a single marine *Synechococcus* clade throughout a stratified water column in
605 the red sea. *Appl Environ Microbiol* 69(5):2430–2443.
- 606 38. Larsson J, et al. (2014) Picocyanobacteria containing a novel pigment gene cluster dominate the
607 brackish water Baltic Sea. *ISME J* 8(9):1892–1903.
- 608 39. Chen F, et al. (2004) Phylogenetic diversity of *Synechococcus* in the Chesapeake Bay revealed by
609 Ribulose-1,5-bisphosphate carboxylase-oxygenase (RuBisCO) large subunit gene (rbcL)
610 sequences. *Aquat Microb Ecol* 36(2):153–164.
- 611 40. Choi DH, Noh JH (2009) Phylogenetic diversity of *Synechococcus* strains isolated from the East
612 China Sea and the East Sea. *FEMS Microbiol Ecol* 69(3):439–448.
- 613 41. Sunagawa S, et al. (2015) Structure and function of the global ocean microbiome. *Science*
614 348(6237):1261359.
- 615 42. Logares R, et al. (2014) Metagenomic 16S rDNA Illumina tags are a powerful alternative to
616 amplicon sequencing to explore diversity and structure of microbial communities. *Environ*
617 *Microbiol* 16(9):2659–2671.
- 618 43. Pearman PB, Guisan A, Broennimann O, Randin CF (2008) Niche dynamics in space and time.
619 *Trends Ecol Evol* 23(3):149–158.
- 620 44. Paulsen ML, et al. (2016) *Synechococcus* in the Atlantic gateway to the Arctic Ocean. *Front Mar*
621 *Sci* 3:191.
- 622 45. Haverkamp THA, et al. (2008) Colorful microdiversity of *Synechococcus* strains
623 (picocyanobacteria) isolated from the Baltic Sea. *ISME J* 3(4):397–408.
- 624 46. Cabello-Yeves PJ, et al. (2017) Novel *Synechococcus* genomes reconstructed from freshwater
625 reservoirs. *Front Microbiol* 8:1151.

- 626 47. Mahmoud RM, et al. (2017) Adaptation to blue light in marine *Synechococcus* requires MpeU,
627 an enzyme with similarity to phycoerythrobilin lyase isomerases. *Front Microbiol* 8:243.
- 628 48. Veldhuis MJW, Kraay GW (1993) Cell abundance and fluorescence of picoplankton in relation to
629 growth irradiance and nitrogen availability in the red sea. *Neth J Sea Res* 31(2):135–145.
- 630 49. Katano T, Nakano S (2006) Growth rates of *Synechococcus* types with different phycoerythrin
631 composition estimated by dual-laser flow cytometry in relationship to the light environment in
632 the Uwa Sea. *J Sea Res* 55(3):182–190.
- 633 50. Ahlgren NA, Rocap G (2006) Culture isolation and culture-independent clone libraries reveal
634 new marine *Synechococcus* ecotypes with distinctive light and N physiologies. *Appl Environ*
635 *Microbiol* 72(11):7193–7204.
- 636 51. Bernal S, Anil AC (2016) Genetic and ecophysiological traits of *Synechococcus* strains isolated
637 from coastal and open ocean waters of the Arabian Sea. *FEMS Microbiol Ecol* 92(11).
- 638 52. Everroad RC, Wood AM (2012) Phycoerythrin evolution and diversification of spectral
639 phenotype in marine *Synechococcus* and related picocyanobacteria. *Mol Phylogenet Evol*
640 64(3):381–392.
- 641 53. Morel A, et al. (2007) Optical properties of the “clearest” natural waters. *Limnol Oceanogr*
642 52(1):217–229.
- 643 54. Cubillos-Ruiz A, Berta-Thompson JW, Becker JW, van der Donk WA, Chisholm SW (2017)
644 Evolutionary radiation of lanthipeptides in marine cyanobacteria. *Proc Natl Acad Sci USA*
645 114(27):E5424–E5433.
- 646 55. Martiny AC, Huang Y, Li W (2009) Occurrence of phosphate acquisition genes in
647 *Prochlorococcus* cells from different ocean regions. *Environ Microbiol* 11(6):1340–1347.
- 648 56. Martiny AC, Coleman ML, Chisholm SW (2006) Phosphate acquisition genes in *Prochlorococcus*
649 ecotypes: evidence for genome-wide adaptation. *Proc Natl Acad Sci USA* 103(33):12552–12557.
- 650 57. Martiny AC, Kathuria S, Berube PM (2009) Widespread metabolic potential for nitrite and
651 nitrate assimilation among *Prochlorococcus* ecotypes. *Proc Natl Acad Sci USA* 106(26):10787–
652 10792.

- 653 58. Katoh K, Standley DM (2013) MAFFT Multiple Sequence Alignment Software Version 7:
654 Improvements in Performance and Usability. *Mol Biol Evol* 30(4):772–780.
- 655 59. Guindon S, et al. (2010) New algorithms and methods to estimate maximum-likelihood
656 phylogenies: assessing the performance of PhyML 3.0. *Syst Biol* 59(3):307–321.
- 657 60. Huerta-Cepas J, Serra F, Bork P (2016) ETE 3: reconstruction, analysis, and visualization of
658 phylogenomic data. *Mol Biol Evol* 33(6):1635–1638.
- 659 61. Camacho C, et al. (2009) BLAST+: architecture and applications. *BMC Bioinformatics* 10:421.
- 660 62. Matsen FA, Kodner RB, Armbrust EV (2010) pplacer: linear time maximum-likelihood and
661 bayesian phylogenetic placement of sequences onto a fixed reference tree. *BMC Bioinformatics*
662 11:538.
- 663 63. R Core Team (2014) *R: A language and environment for statistical computing* (R Foundation for
664 Statistical Computing, Vienna, Austria) Available at: <http://www.R-project.org/>.
- 665 64. Maechler M, Rousseeuw P, Struyf A, Hubert M, Hornik K (2017) *cluster: cluster analysis basics
666 and extensions*.
- 667 65. Venables WN, Ripley BD (2002) *Modern applied statistics with S* (Springer, New York). Fourth
668 edition. Available at: <http://www.stats.ox.ac.uk/pub/MASS4>.
- 669 66. Harrell FE (2016) *Hmisc: Harrell Miscellaneous* Available at: [http://CRAN.R-
670 project.org/package=Hmisc](http://CRAN.R-project.org/package=Hmisc).

671

672

673 **Legends of Figures**

674 **Fig. 1:** Maximum likelihood phylogenetic trees of (A) *cpcBA* operon, (B) *mpeBA* operon and (C) the
675 *mpeW/Y/Z* gene family. The *cpcBA* tree includes both strains with characterized pigment type (PT)
676 and environmental sequences (prefixed with GS) assembled from metagenomes of the Baltic Sea
677 (38). Circles at nodes indicate bootstrap support (black: > 90 %; white: > 70 %). Note that for PT 2B
678 clade, only environmental sequences are available. The PT associated with each sequence is
679 indicated as a colored square. The scale bar represents the number of substitutions per nucleotide
680 position.

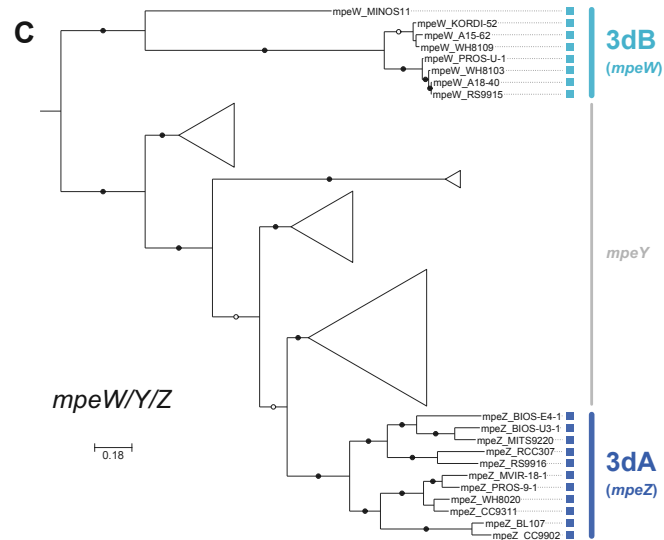
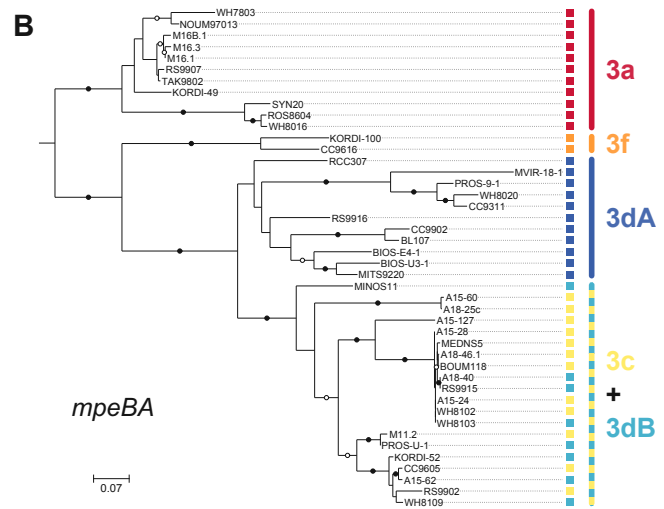
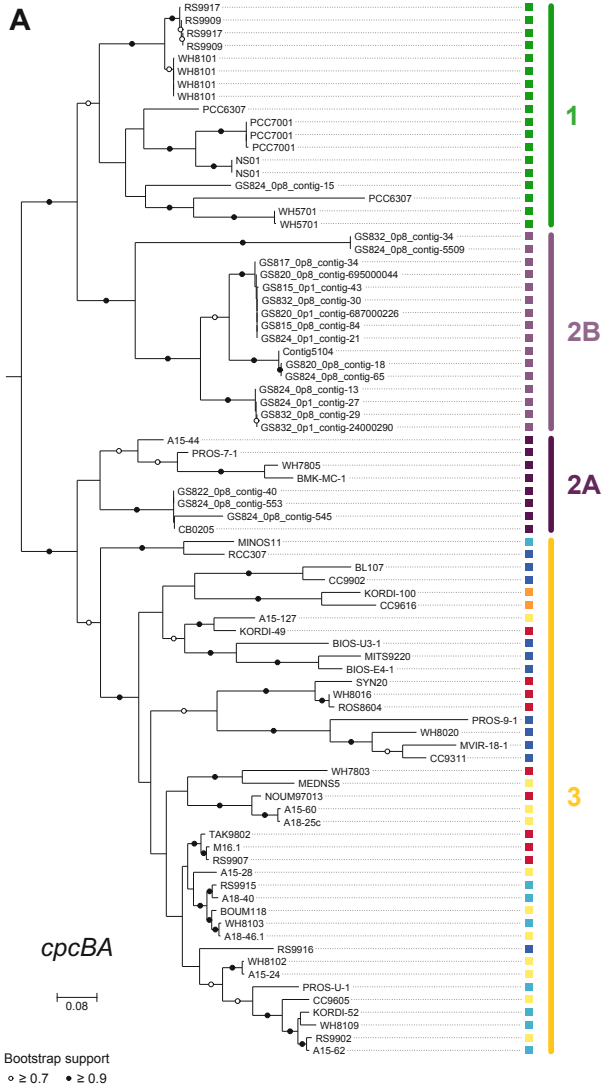
681

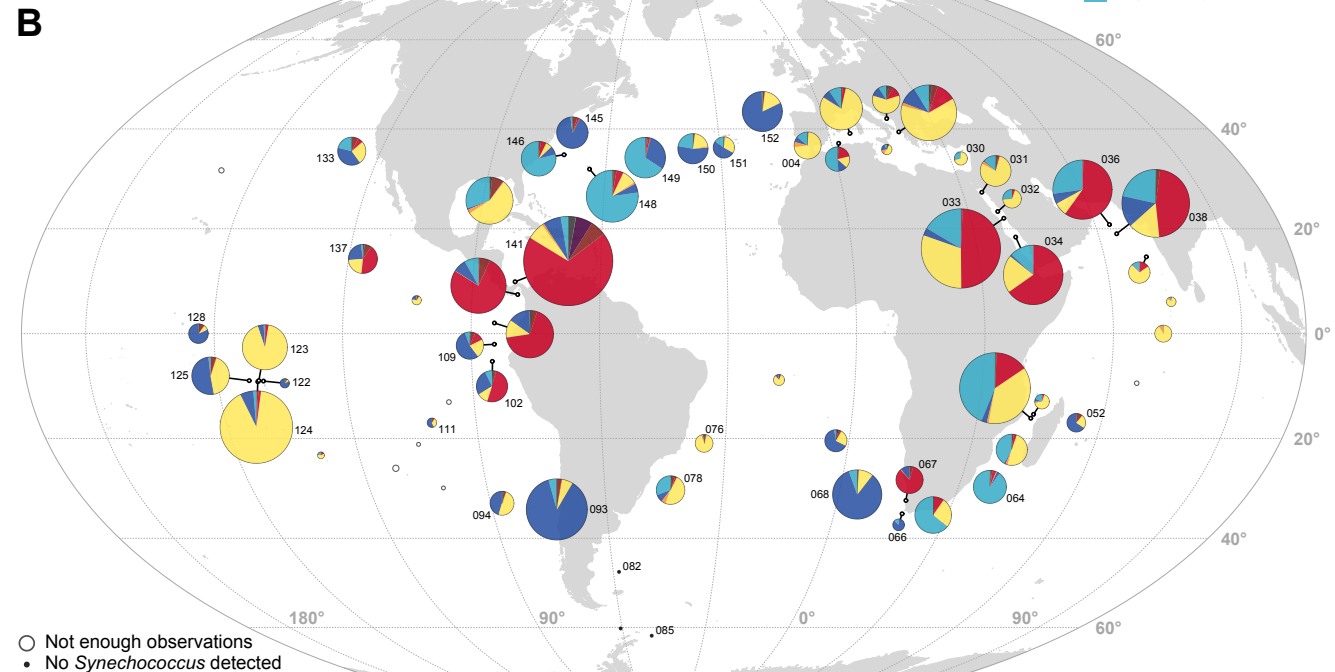
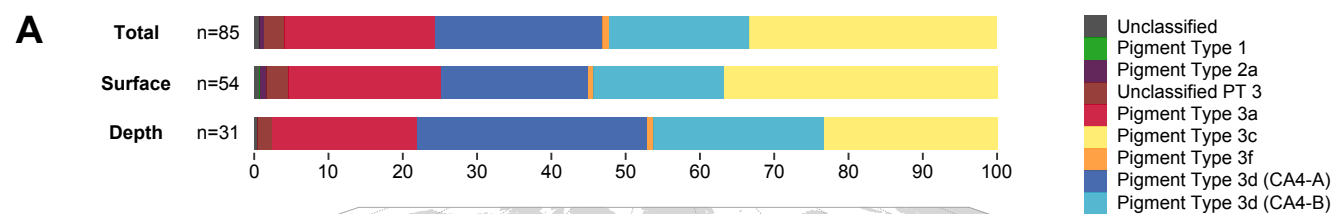
682 **Fig. 2:** Distribution of *Synechococcus* pigment types (PT). (A) Relative abundance of each PT in the
683 whole dataset (Total), in surface and at the DCM (Deep Chlorophyll Maximum). (B) Map showing the
684 global distribution of all *Synechococcus* PTs in surface waters along the *Tara* Oceans transect.
685 Diameters of pies are proportional to the number of *cpcBA* reads normalized by the sequencing
686 effort. Stations with less than 30 *cpcBA* or *mpeBA* reads are indicated by open circles and those with
687 no *cpcBA* reads by black dots. Numbers next to pies correspond to *Tara* Oceans stations.

688

689 **Fig. 3:** Correlation analysis between *Synechococcus* pigment types (PT) and environmental
690 parameters measured along the *Tara* Oceans transect for all sampled depths. The scale shows the
691 degree of correlation (blue) or anti-correlation (red) between two variables. Non-significant
692 correlations (adjusted *P* value > 0.05) are indicated by crosses. Number of observations for each
693 environmental parameter is indicated at the bottom. Abbreviations: MLD, mixed layer depth; DCM,
694 deep chlorophyll maximum; IS, *in situ*; Backscatt., backscattering; part., particulate; cDOM fluo,
695 colored dissolved organic matter fluorescence; BAC, beam attenuation coefficient; Φ_{sat} , satellite-
696 based non-photochemical quenching (NPQ)-corrected quantum yield of fluorescence (proxy for iron
697 limitation; 6); PAR, photosynthetically active radiation; NPP, net primary production; $I_{\text{rr}}_{495:545}$, ratio of
698 downwelling irradiance at 495 nm and 545 nm.

700 **Fig. 4:** Relationship between *Synechococcus* pigment types (PT) and Ecologically Significant
701 Taxonomic Units (ESTUs, as defined in 6). (A) Correlation analysis between *Synechococcus* PTs and
702 the most abundant ESTUs (>1% relative abundance) for all sampled depths (the complete dataset is
703 shown in Fig. S5). Non-significant correlations (adjusted *P* value > 0.05) are indicated by crosses. The
704 surface of station TARA_067, identified as an outlier (see Fig. S7), was removed for this analysis. (B)
705 NMDS analysis of stations according to Bray–Curtis distance between PT assemblages. Samples that
706 belong to the same ESTU assemblage have been contoured with a background color according to the
707 color code used in (6), namely: red, assemblage 1 dominated by ESTU IIA; yellow, assemblage 2
708 dominated by ESTU IIIA; dark blue, assemblage 4 dominated by ESTUs IA and IVA/B; pink, assemblage
709 5 co- dominated by ESTUs IIB and IVA/B; grey, assemblage 6 co-dominated by ESTUs CRD1C and
710 EnvBC; light blue, assemblage 8 co-dominated by ESTUs IVA/B, EnvBB and CRD1A/B. (C) PT and ESTU
711 relative abundance at each surface station along the *Tara* Oceans transect. Oceanic provinces are
712 indicated in the top gray panels. NAO, North Atlantic Ocean; MS, Mediterranean Sea; RS, Red Sea; IO,
713 Indian Ocean; SAO, South Atlantic Ocean; SO, Southern Ocean; SPO, South Pacific Ocean; NPO, North
714 Pacific Ocean.





Physical parameters

Chemical parameters

Optical parameters

Temperature

Conductivity

Salinity

Density

ML depth

DCM depth

Nitracline depth

Fe

 NH_4^+ NO_3^- NO_2^- $\text{NO}_3^- + \text{NO}_2^-$ H_3PO_4 $\text{Si}(\text{OH})_4$

Chlorophyll a (IS)

Backscatt. 470nm

Backscatt. 470nm

cDOM fluo. (IS)

cDOM fluo. (part.)

BAC 660nm

BAC 660nm (part.)

 ϕ_{sat}

PAR

NPP

 $\text{Irr}_{495-545}$

2A

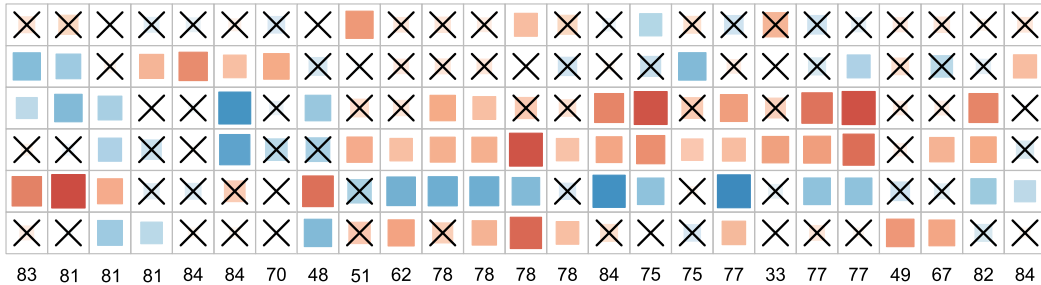
3a

3c

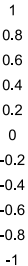
3f

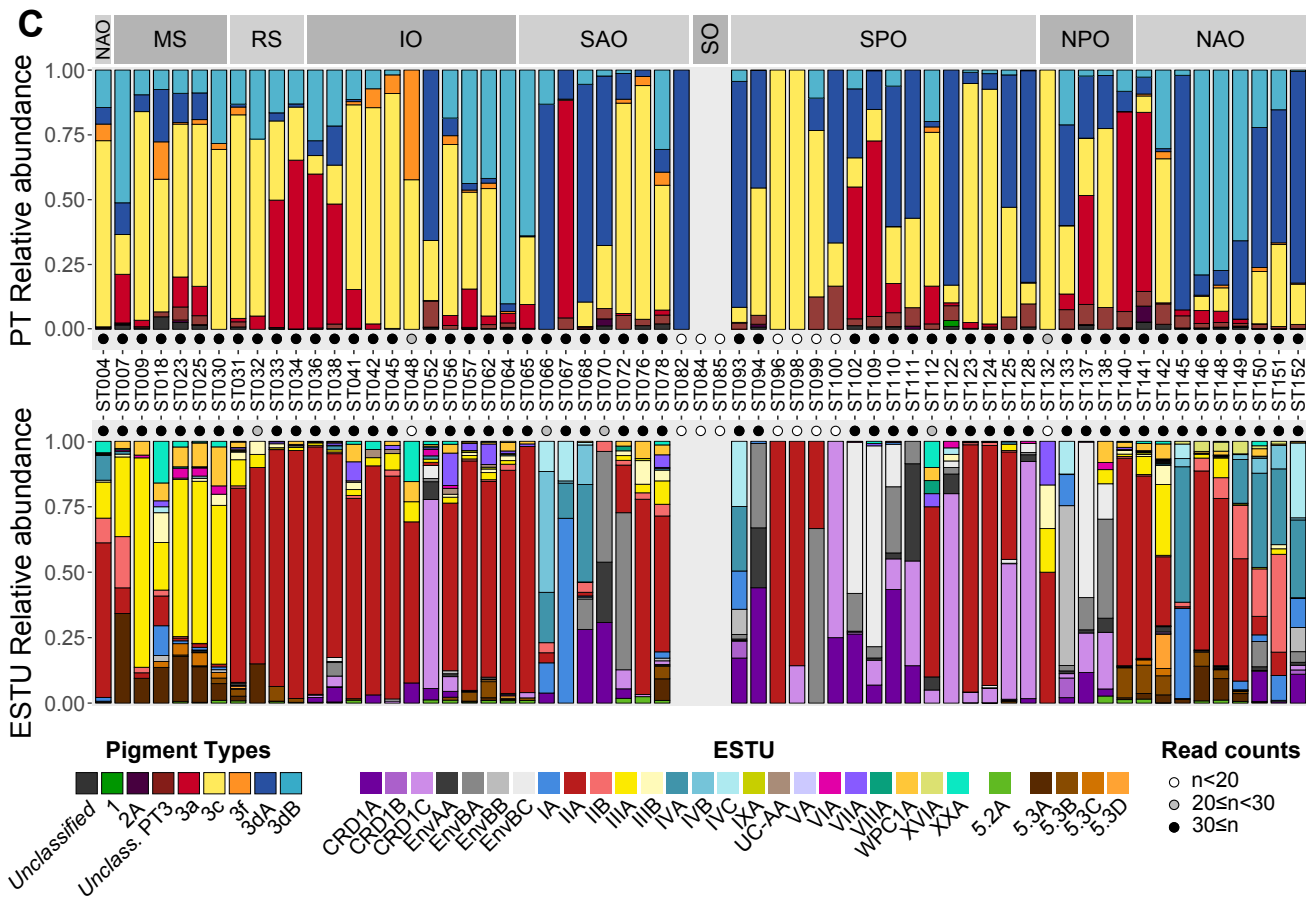
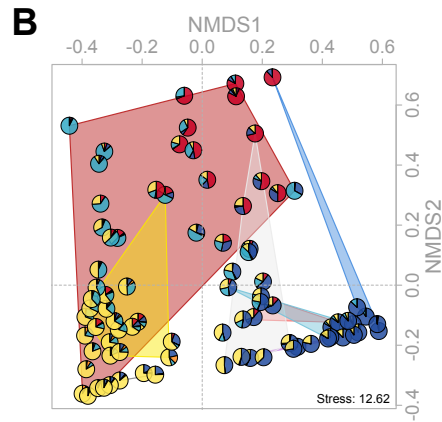
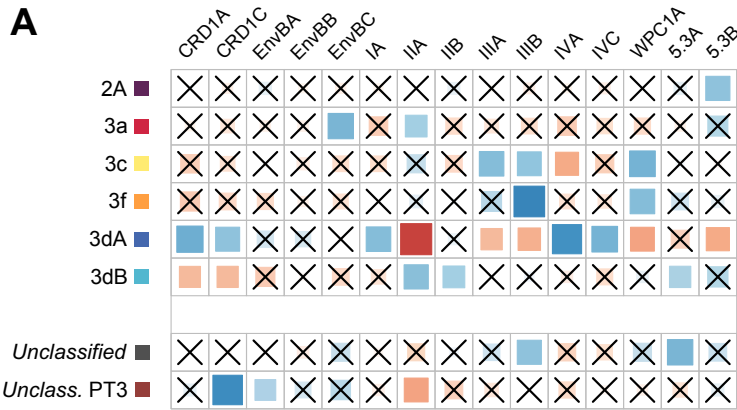
3dA

3dB



Spearman's rho





Supplementary materials and methods

Modeling of the blue to green irradiance ratio ($Irr_{495:545}$) at *Tara* Oceans stations.

We used the clear sky surface irradiance model of Frouin and McPherson in Fortran and translated to Matlab by Werdell (see Frouin et al., 1989 and Tanre et al., 1979 for the analytical formula used) using the date, latitude and longitude of each station, assuming sunny sky and at noon.

The spectral light distribution averaged over the mixed layer was computed from:

$$\langle Ir(\lambda) \rangle = \frac{\int_0^{MLD} E(\lambda, 0^-) e^{-k(\lambda, chl)z} dz}{MLD} = \frac{I(\lambda, 0^-)}{MLD k(\lambda, chl)} \{1 - e^{-k(chl)MLD}\}$$

where:

- *chl* denotes the average chlorophyll value in the mixed layer. [*chl*] was based on a fluorometer that was calibrated against HPLC data and corrected for non-photochemical quenching,
- MLD is the mixed layer depth that was computed based on a temperature threshold criterion
- $k(\lambda, chl)$ is the diffuse attenuation coefficient at wavelength λ (495 or 545 using a 10 nm bandwidth). This parameter was computed using Morel and Maritorena (2001)'s equation:

$$k(\lambda, chl) = k_w(\lambda) + \chi(\lambda)[chl]^{e(\lambda)}$$

k_w , χ and e are provided in Table 2 of Morel and Maritorena (2001) and have the following values for the wavelengths of interest:

Wavelength [nm]	$k_w(\lambda)$ [m^{-1}]	$\chi(\lambda)$	$e(\lambda)$
495	0.01885	0.06907	0.68947
545	0.05212	0.04253	0.65591

If the sampling depth was below the MLD, the irradiance was computed as follows:

$$Ir(\lambda, sampling\ depth) = I(\lambda, 0^-) e^{-k(\lambda, chl) sampling\ depth}$$

The ratio was then computed as $Irr_{495:545}$.

References:

- Frouin, R., D. W. Ligner, and C. Gautier, 1989: A Simple analytical formula to compute clear sky total and photosynthetically available solar irradiance CC at the ocean surface. *J. Geophys. Res.*, 94, 9731-9742.
- Morel, A. and S. Maritorena, 2001: Bio-optical properties of oceanic waters: A reappraisal. *J. Geophys. Res.*, 106, 7163–7180.

Tanre, D., M. Herman, P.-Y. Deschamps, and A. De Leffe, 1979: Atmospheric modeling for Space measurements of ground reflectances, including bi-directional properties. *Appl. Optics*, 18, 21,3587-21,3597.

Legends to supplementary figures

Figure S1: Biochemical composition and biooptical properties of phycobilisomes (PBS) of the main *Synechococcus* pigment types (PT). (A) Models of PBS structure, highlighting the conserved core and variable rods of increasing complexity from PT1 to PT3 (Redrawn after Six *et al.*, 2007). (B) Whole cell absorption spectra of the different PTs (Reproduced after Six *et al.*, 2007). Chromophores responsible of each absorption peaks are indicated. (C) Whole cell fluorescence excitation spectra with emission at 680 nm. Note that for chromatic acclimators (PT 3d), the PBS structure is similar to other PT 3 but that the excitation ratio at 495 nm and 545 nm ($Ex_{495:545}$) varies from 0.6 in green light to 1.6 in blue light (not shown).

Figure S2: Evaluation of the assignment pipeline and the resolution power of the different markers used in this study. Simulated reads were generated from the reference dataset and assigned using a custom-designed pipeline (see materials and methods). (A, C, E) Evaluation of different sets of parameters tested for read assignment for the different markers: *cpcBA* (A), *mpeBA* (C) and *mpeW* (E). 100 (yellow), 125 (pink) and 150 bp (dark red) long reads were simulated. For each read, pplacer returns a list of possible positions in the tree, each associated with a likelihood weight. From these placements, we considered only those that reached a summed likelihood weight of either 90% (circle), 95% (square) or 100% (triangle). The assignment was then performed based on the phenotype of either the nearest node (solid symbol) in the tree or the descending (child) node (empty symbol). (B, D, F) Evaluation the resolution power along *cpcBA* (B), *mpeBA* (D) or *mpeW* (F) for 150 bp simulated reads assigned using the parameters selected for *Tara Oceans* metagenomic read assignment (i.e., nearest node assignment and summed weight of 95%). Note that *Tara Oceans* reads had a mean length of 164 bp.

Figure S3: Correlations between the number of reads recruited using the main markers used in this study. (A) Correlation between *petB* (vertical phylogeny) and *cpcBA* counts used to discriminate pigment types (PT) 1, 2 and 3. (B) Correlation between PT 3 counts using *cpcBA* and total *mpeBA* counts. Note that *mpeBA* is a PT3 specific marker and is used to discriminate PTs 3a, 3dA, 3f and 3c+3dB. (C) Correlation between PT 3dB counts using *fciAB*, a PT 3dB- and 3dA-specific marker and total *mpeW* counts, a PT 3dB-specific marker.

Figure S4: Distribution of *Synechococcus* pigment types (PTs) at depth (Deep Chlorophyll Maximum). (A) Map showing the global distribution of all *Synechococcus* PTs at depth along the *Tara* Oceans transect. Diameters of pies are proportional to the number of *cpcBA* reads normalized by the sequencing effort. Stations with less than 30 *cpcBA* or *mpeBA* reads are indicated by open circles and those with no *cpcBA* reads by black dots. Numbers next to pies correspond to *Tara* Oceans stations. (B) PTs and ESTU relative abundance at depth for sampling station along the *Tara* Oceans transect. Oceanic provinces are indicated in the top gray panels. NAO, North Atlantic Ocean; MS, Mediterranean Sea; RS, Red Sea; IO, Indian Ocean; SAO, South Atlantic Ocean; SO, Southern Ocean; SPO, South Pacific Ocean; NPO, North Pacific Ocean.

Figure S5: Same as Fig. 4A but for all ESTUs. Unclass., unclassified.

Figure S6: Focus on pigment type (PT) 3dA natural mutants, exhibiting an altered gene content with regard to typical PT 3dA. (A-J) Correlation between the number of reads assigned as PT 3dA using different markers (all present in single gene copy in typical 3dA). Each circle corresponds to a *Tara* Oceans station and depth. Orange circles: stations with at least 20 *mpeBA* reads assigned to PT 3dA and at least twice more 3dA counted with *mpeBA* than with *fciAB*, corresponding to the surface sample of stations TARA_070, TARA_110 and TARA_137 and the

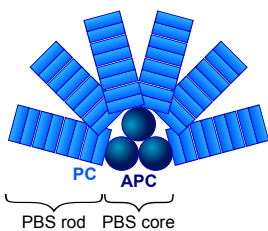
DCM of stations TARA_038, TARA_058 and TARA_110. Red circles: same but with more than 10-fold 3dA counted with *mpeBA* than *fciAB*, corresponding to the surface sample of stations TARA_052, TARA_094, TARA_111 and TARA_122 to TARA_128, and DCM of stations TARA_052, TARA_100, TARA_111 and TARA_128. Green circle: surface of station TARA_067. (K) CA4-A genomic island and fragment of the phycobilisome (PBS) genomic region for a typical, CA4-able 3dA strain (strain BL107), and 3 CA4-deficient strains, which are stuck either in blue light phenotype (similar to strain BIOS-E4-1), or green light phenotype (as strains MVIR-18-1 and WH8016). Note that KORDI-49 and WH8016 strains have identical PBS gene complement and genomic arrangement. The complete PBS genomic region of the BL107 strain can be found in Six *et al.*, 2007. Note that for readability, surface of station TARA_093 has been omitted since it has the highest normalized counts (2.7-3.2) for all markers and exhibited a good agreement between markers (ratio close to 1:1).

Figure S7: Correlation between the proportion of clades I, IV and CRD1, as assessed with *petB*, and the proportion of pigment type 3dA, as assessed with *mpeBA*, at each station.

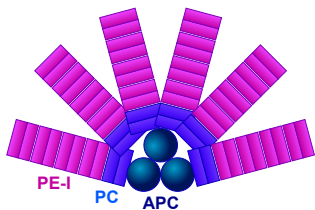
A

Model of PBS structure

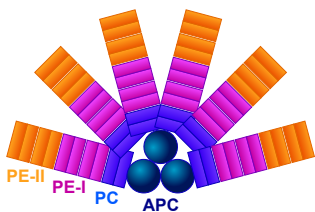
Pigment Type 1 ■



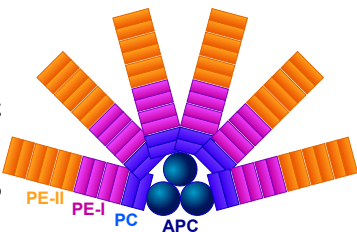
Pigment Type 2 ■



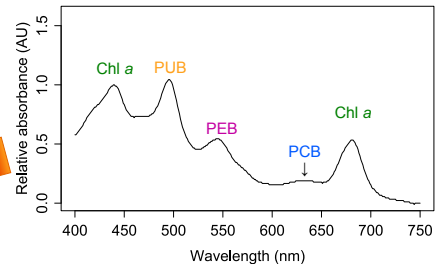
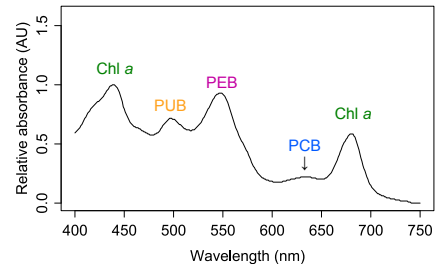
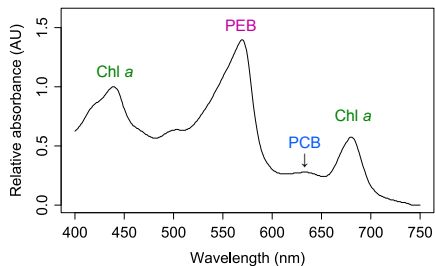
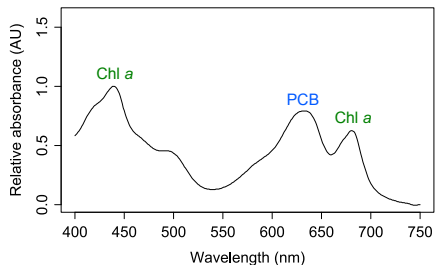
Pigment Type 3a ■



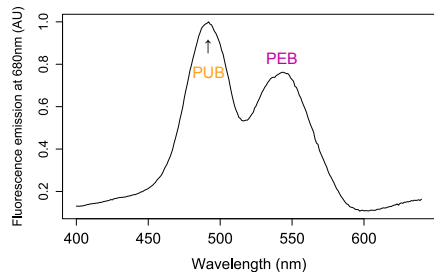
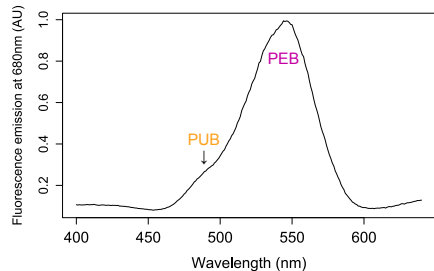
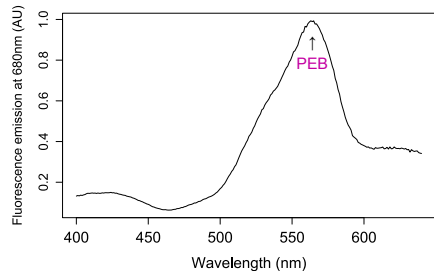
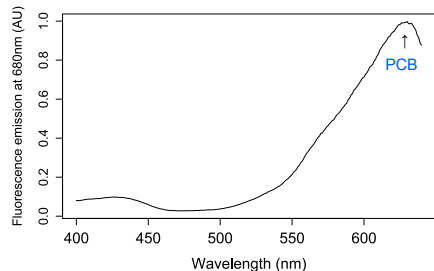
Pigment Type 3c ■

**B**

Whole cell absorption spectra

**C**

Whole cell fluorescence excitation spectra



Phycobiliproteins

- APC Allophycocyanin
- PC Phycocyanin
- PE-I Phycoerythrin-I
- PE-II Phycoerythrin-II

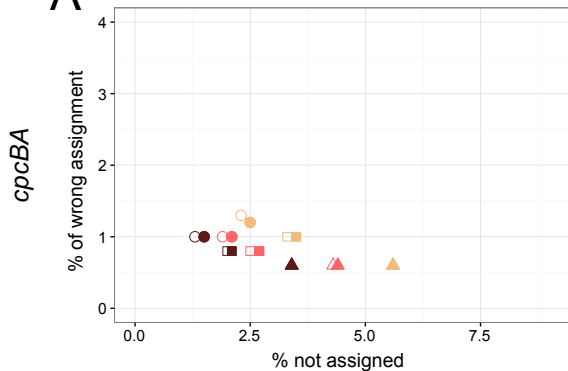
Phycobilins

- PCB Phycocyanobilin ($A_{\max} = 620 \text{ nm}$)
- PEB Phycoerythrobin ($A_{\max} = 545\text{-}560 \text{ nm}$)
- PUB Phycourobilin ($A_{\max} = 495 \text{ nm}$)

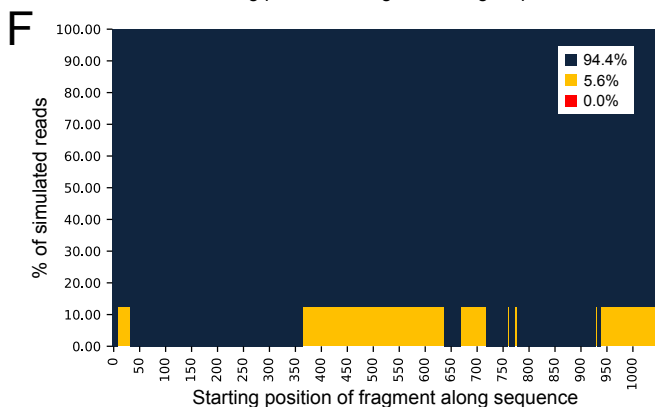
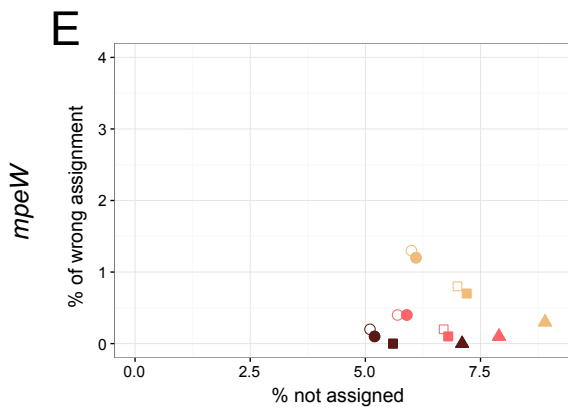
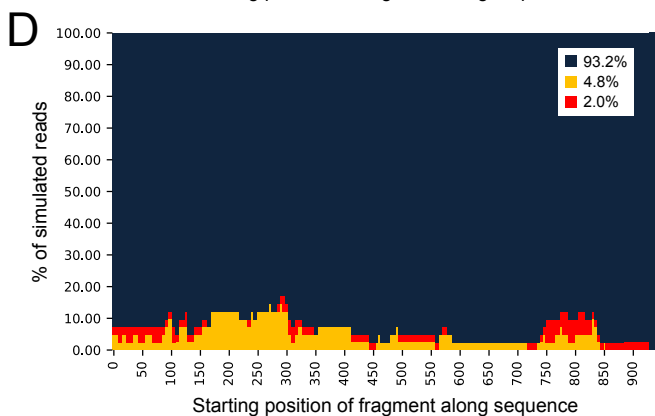
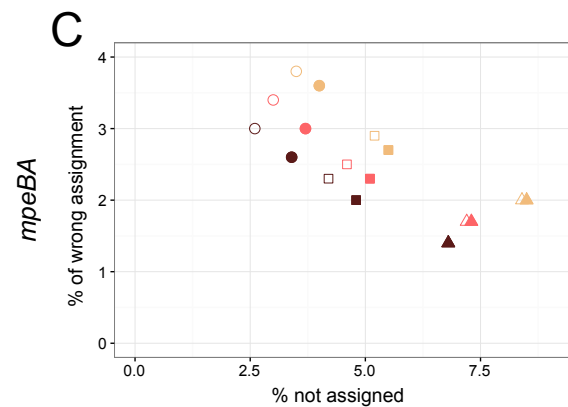
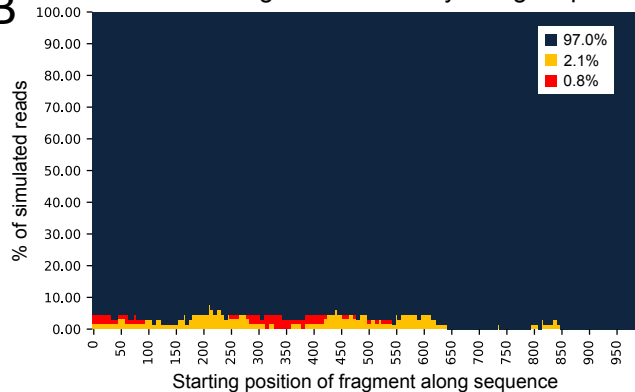
Other chromophore

- Chl a Chlorophyll a

A Evaluation of parameters sets



B Evaluation of assignment accuracy along sequence



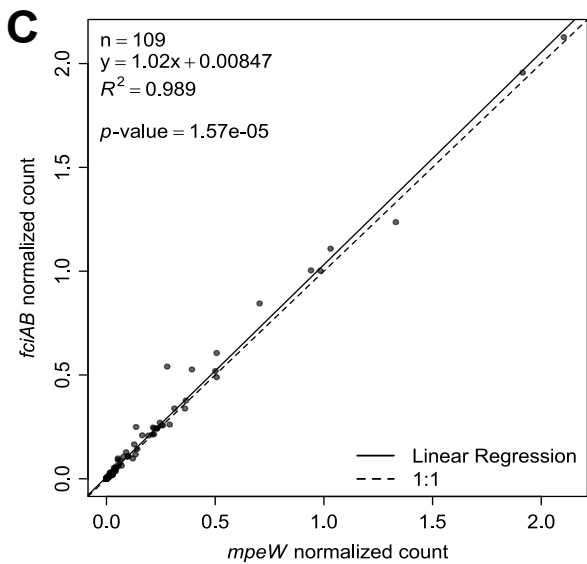
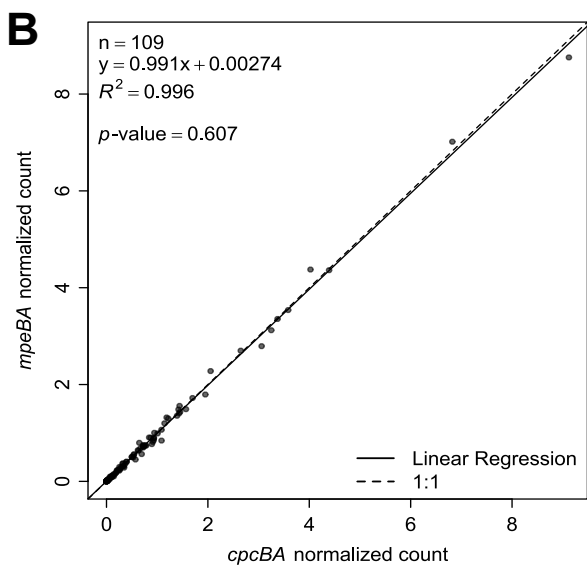
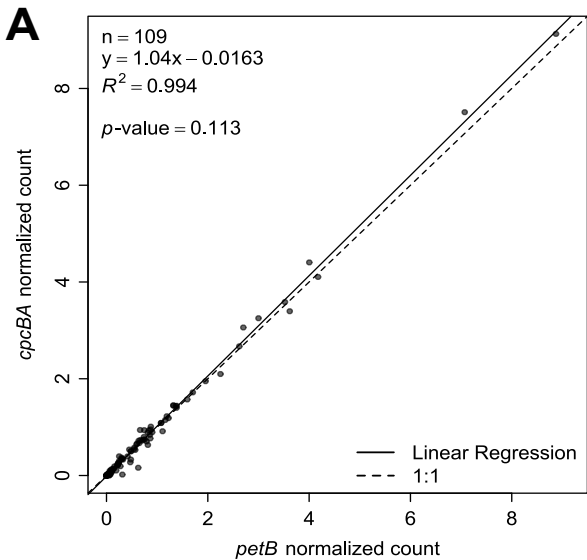
Simulated read length Summed weight Node assignment

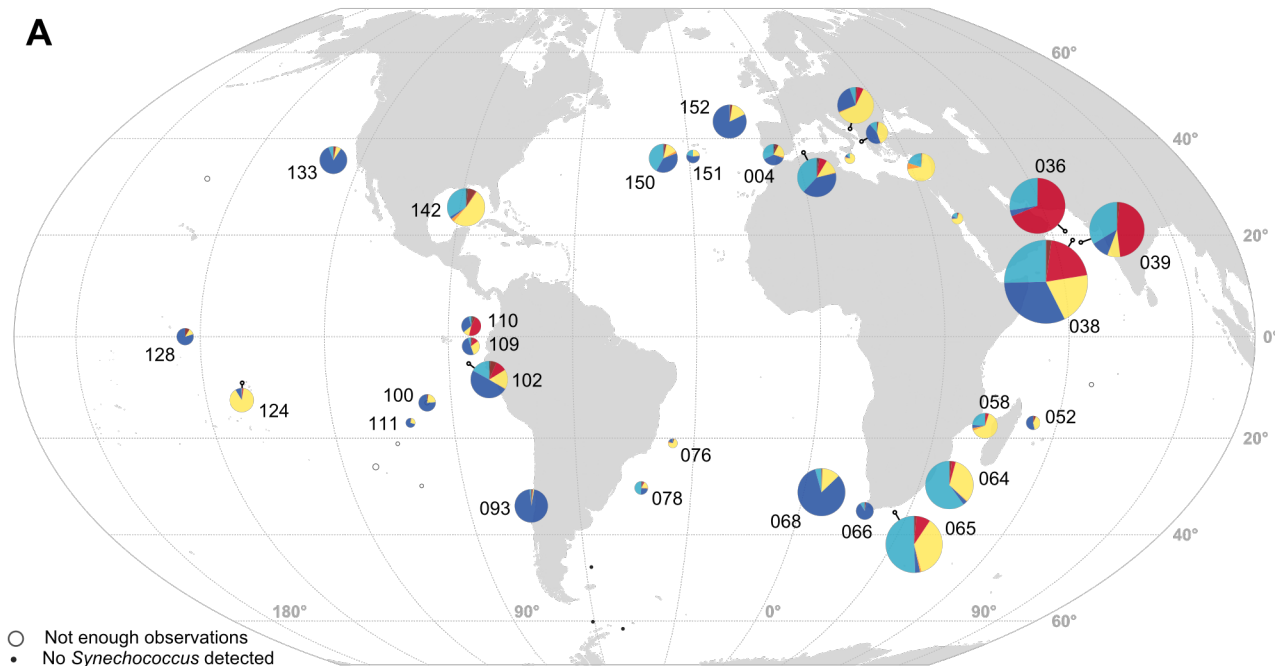
● 100 bp ○ 90% ● Nearest

● 125 bp □ 95% ○ Descending

● 150 bp △ 100%

■ Correct assignment ■ Not assigned ■ Wrong assignment



A**B**